J Mater Sci (2013) 48:979–988
DOI 10.1007/s10853-012-6713-7

REVIEW

Thermo-mechanical and fracture properties in single-crystal silicon

Alex Masolin · Pierre-Olivier Bouchard · Roberto Martini · Marc Bernacki

Received: 14 May 2012 / Accepted: 2 July 2012 / Published online: 18 July 2012

Abstract Single-crystal silicon is extensively used in the semiconductor industry. Even though most of the steps during processing involve somehow thermo-mechanical treatment of silicon, we will focus on two main domains where these properties play a major role: cleaving techniques used to obtain a thin silicon layer for photovoltaic applications and MEMS. The evolution and validation of these new processes often rely on numerical simulations. The accuracy of these simulations, however, requires accurate input data for a wide temperature range. Numerous studies have been performed, and most of the needed parameters are generally available in the literature, but unfortunately, some discrepancies are observed in terms of measured data regarding fracture mechanics parameters. The aim of this article is to gather all these data and discuss the validity of these properties between room temperature and 1273 K. Particular attention is given to silicon fracture properties depending on crystallographic orientations, and to the brittle–ductile temperature transition which can strongly affect the quality of silicon layers.

A. Masolin · R. Martini
KU Leuven, Oude Markt 13, 3000 Leuven, Belgium

A. Masolin (✉) · R. Martini
Imec, Kapeldreef 75, 3000 Leuven, Belgium
e-mail: alex.masolin@imec.be

P.-O. Bouchard · M. Bernacki
Mines ParisTech, CEMEF-Centre de Mise en Forme des Matériaux, CNRS UMR 7635, BP 207, 1 rue Claude Daunesse, 06904 Sophia Antipolis Cedex, France

Introduction

Nowadays silicon is the most employed material in semiconductor industry. Integrated circuits, solar cells and micro-electromechanical systems (MEMS) industries extensively use this material both as single-crystal silicon (also called monocrystalline silicon), which consists of silicon where the crystal lattice of the entire solid is continuous, with no misorientation, and polycrystalline, which consists of a collection of grains of single-crystal silicon separated by grains boundaries. Because of its wide use, silicon properties have been thoroughly investigated in the past from an electrical and mechanical point of view.

In the last decades, thermo-mechanical properties of single-crystal silicon have gained more and more interest due to its use in solar cell and MEMS industries. Common processes in these industries involve very high temperatures and an assessment of both stresses induced in silicon during these processes and the residual stresses after the processes is paramount to analyze the feasibility of these processes without breaking the sample. MEMS are sensors and actuators where sensing or actuating parts consist of micrometers-scaled structures, e.g., cantilevers, bridges and plates, usually made of silicon. The mechanical properties of these microstructures have to be tailored and the residual stresses after the fabrication have to be assessed to design MEMS with certain properties. A considerable number of papers have been published on the design of MEMS which cover a wide range of MEMS, such as microphones, accelerometers, pressure sensors, switches, and micro-grippers. In the solar cell industry, mechanical properties of silicon are important to estimate the final bowing of very thin wafers after the contact formation. Further interest in mechanical properties of silicon and, more precisely, in its post-elastic behavior at very different

temperature is due to the cleaving technology to manufacture thin silicon foils. Various new experimental techniques have been proposed to produce such thin silicon wafers without kerf loss [1].

Applications exist where the thermo-mechanical and fracture properties of silicon are changed in order to obtain a weak layer, such as [2, 3]. Since the presence of such weak layers inherently changes the thermo-mechanical properties of bulk silicon, they will not be reviewed in this paper.

The first work reported in literature about cleaving silicon wafer by using pure thermo-mechanical properties dates from 1975 [4]. This patent describes an idea on how to control the propagation of a crack in crystalline materials to produce thin wafers. The first step is to introduce a preselected stress concentration into the crystal, e.g., by means of a notch or a scribe line. Subsequently an internal tensile stress, acting in normal direction, may be accomplished by tensile, compressive, shear forces or by a bending or torsional moment. Finally, the fracture can be achieved, e.g., by a wedge, expanding material in the notch, a stress wave, and impact load.

Later, at the beginning of the eighties, Wilkes [5] proposed a process for cleaving boules of single crystal material by creating an inward-directed radial stress concentration completely around a boule which intersects its crystallographic plane of minimum bond strength. Then, triggering the cleavage via a shock wave applied.

Tanielian et al. [6] proposed a method to produce foils by sputtering deposition of a layer of metal onto a single crystal substrate. Then, the assembly is treated to stress the metal layer which then can peel off with a part of the single crystal substrate still attached. Free standing foils thus produced have typical thicknesses in the order of tens of micrometers.

A few years later, Owens [7, 8] and Takeguchi [9] invented a tool to cleave brittle materials into thin sections using the same principle of the aforementioned Hillberry [4], namely the use of a wedge to induce a pure opening mode into the crystal.

Almost two decades later, Yamaguchi [10] re-proposed to cleave a wafer from an ingot in a two-step approach: generation of a line defect on the surface by means of ion beam along a direction defined by crystal axes and then cleaving the ingot applying a shock in the same point by means of a knife-edge. A few years later, Baer [11] chose a two-step process, where the first is the creation of a notch at a given depth. The crack is propagated then by applying light at a wavelength absorbed at the same given depth of a notch. The heat generated by absorption of such light, which is scanned along the desired direction, is claimed to be sufficient to propagate the crack.

Dross et al. [12–14] presented the SLIM-cut process, which consists in inducing a tensile stress in the silicon substrate in order to initiate [15] and to propagate a crack at a given depth . In order to generate such a tensile stress field, a metallic stress-inducing layer is deposited and the system brought at high temperature. During the cooling stage, the mismatch between the coefficient of thermal expansion (CTE) of the metal and the silicon induces a tensile stress field that can be high enough to initiate and propagate a crack all along the silicon substrate [16]. The temperature range in which lift-off occurs in the SLIM-cut process, may include the silicon brittle–ductile transition temperature: specific attention to this brittle–ductile temperature transition must be paid if one wants to obtain sound defect-free silicon layer after fracture [17, 18]. Alternatively, the stress-inducing layer can also be a polymer-based material, where the process involves a much lower thermal budget and peak temperatures, assuring brittle crack propagation [19].

A company [20, 21] is marketing solar cells using the same principle meanwhile also IBM [22–24] claims being able to produce multiple high quality thin silicon layers from a single substrate.

The set up and optimization of the aforementioned manufacturing processes imply the use of numerical modeling, which in turns requires accurate input data in terms of thermo-mechanical behavior of silicon. A considerable number of papers have been published about thermo-mechanical properties and fracture properties of silicon, but they are spread all over the literature and they sometimes contradict each other. In this article, the mechanical properties of single-crystal silicon between 293 and 1273 K will be firstly presented and discussed, "Mechanical properties of single-crystal silicon" section will focus on its thermal properties in the same temperature range, while "Thermal properties of single-crystal silicon" section will discuss about the fracture properties of single-crystal silicon.

Mechanical properties of single-crystal silicon

Silicon, like carbon and germanium, crystallizes at common pressures in a diamond cubic crystal structure with a density of 2.329 g cm^{-3} at 298 K. Therefore, silicon is an anisotropic material whose properties depend on its relative orientation to the crystal lattice as well as an orthotropic material, i.e., a crystal with at least two orthogonal planes of symmetry. Silicon is a brittle material at room temperature, which means that its behavior is purely elastic until failure.

Elastic constants

In an anisotropic material, Hooke's law involves a fourth rank tensor (either the stiffness C or the compliance S) to

describe the elastic relationship between the second rank stress σ and strain ε tensors:

$$\sigma_{ij} = C_{ijkl}\varepsilon_{ij} \quad \text{and} \quad \varepsilon_{ij} = S_{ijkl}\sigma_{kl}. \tag{1}$$

In silicon, the combination of cubic symmetry and the equivalence of the shear conditions enable specifying the fourth rank tensor with only three independent elastic constants. These tensors are given with respect to a specific basis, which in the case of the cubic structure of silicon is commonly given for the $\langle 100 \rangle$ directions.

$$\begin{aligned} \sigma_{ii} &= C_{11}\varepsilon_{ii} + C_{12}(\varepsilon_{jj} + \varepsilon_{kk}) \\ \sigma_{ij} &= C_{44}\varepsilon_{ij} \end{aligned} \tag{2}$$

The tensor can then be easily rotated in the orientation of interest. Up to now, the best measurement of the elastic constant is achieved using acoustic wave propagation in the solid. Even if the values from Mason [25] are often cited in the literature, the measurement performed a decade later by Hall [26] reports slightly better accuracy (Table 1).

In the context of orthotropic materials, as for silicon, it is possible to give, for the axes of interest, the elastic properties in terms of orthotropic material constants involving the Young's modulus E, the Poisson's ratio n, and the shear modulus G.

The Young's modulus is a parameter to characterize the stiffness of an elastic material. It can be measured from the slope of the linear portion of the stress–strain curve recorded from an experiment where the specimen undergoes to a uniaxial load.

Otherwise the Young's modulus E can be calculated from the general formulae for cubic crystal [27]:

$$\frac{1}{E_{hkl}} = S_{11} - 2\left[S_{11} - S_{12} - \frac{1}{2}S_{44}\right]\left(m^2n^2 + p^2n^2 + m^2p^2\right), \tag{3}$$

where m, n, p are the "direction cosines", i.e., the cosine of the angle between the $[hkl]$ direction and the three basis axes (the $\langle 100 \rangle$ directions). For a better understanding, three different cases, at room temperature, are illustrated in the Table 2 where a classical [110] direction is assumed for the primary flat. The first column corresponds to the case where the used basis is equal to the $\langle 100 \rangle$ directions and so, for each subscript x, y, or z, two of the "direction cosines" are null. Therefore,

$$E_x = E_y = E_z = 1/S_{11} \approx 130\,\text{GPa}. \tag{4}$$

For the second column, the subscript x (resp. y) corresponds to the [110] (resp. $[\bar{1}10]$) directions. Therefore,

Table 1 Elastic constants of silicon at 298 K (C: 10^9Pa, S: 10^{-12}Pa)

C_{11}	C_{12}	C_{44}	S_{11}	S_{12}	S_{44}
165.64	63.94	79.51	7.69	−2.14	12.6

Table 2 Approximate values of elasticity in the reference frame of standard silicon wafers

Wafer (GPa)	(100)		(111)
	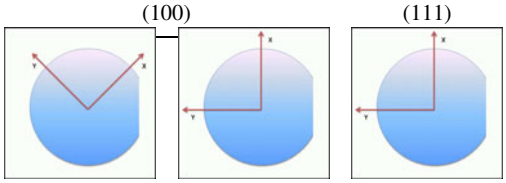		
E_x	130	169	174
E_y	130	169	174
E_z	130	130	188
ν_{yz}	0.278	0.362	0.166
ν_{zx}	0.278	0.362	0.166
ν_{xy}	0.278	0.064	0.241
G_{yz}	79.6	79.6	60.5
G_{zx}	79.6	79.6	60.5
G_{xy}	79.6	50.9	70.0

$$\begin{aligned} E_x = E_y &= \left(S_{11} - 2\left(S_{11} - S_{12} - \frac{1}{2}S_{44}\right)\left(\frac{1}{\sqrt{2}}\right)^2\left(\frac{1}{\sqrt{2}}\right)^2\right)^{-1} \\ &= 2\left(S_{11} + S_{12} + \frac{1}{2}S_{44}\right)^{-1} \approx 169\,\text{GPa} \end{aligned} \tag{5}$$

$$E_z = 1/S_{11} \approx 130\,\text{GPa} \tag{6}$$

Same methodology can be used for the third column in the context of a (111) wafer. Brantley et al. [28] reports maximum and minimum values of Young's modulus for other directions lying in important crystal planes. Concerning Poisson's ratio and shear modulus, the cubic crystal configuration allows also using the following formulae:

$$\upsilon_{\alpha\beta} = \frac{S_{12} + \left[S_{11} - S_{12} - \frac{1}{2}S_{44}\right]\left(m_\alpha^2 m_\beta^2 + n_\alpha^2 n_\beta^2 + p_\alpha^2 p_\beta^2\right)}{S_{11} - 2\left[S_{11} - S_{12} - \frac{1}{2}S_{44}\right]\left(m_\alpha^2 n_\alpha^2 + p_\alpha^2 n_\alpha^2 + m_\alpha^2 p_\alpha^2\right)} \tag{7}$$

$$G_{ij} = 1/S_{ij} \tag{8}$$

with α and β two orthogonal directions, and m_γ, n_γ, p_γ, , the "direction cosines" of the angle between the γ direction and the basis axes.

Finally, the bulk modulus B can be also obtained from:

$$B = \frac{C_{11} + 2C_{12}}{3}. \tag{9}$$

At room temperature (298 K), these formula leads to a bulk modulus B of 0.9781×10^{11}Pa (therefore a compressibility K of $1.0221 \times 10^{-11}\text{Pa}^{-1}$), which is in very good agreement with $B \sim 0.995 \pm 0.005 \times 10^{11}$ Pa measured in real experiments [29, 30]. The values of the Poisson's ratio and shear modulus for the different configurations considered are summarized in Table 2.

Table 3 Temperature coefficients of the elastic constants

TCE	First-order ($\times 10^{-6}$/K)		Second-order ($\times 10^{-6}$/K)	
	p-type 4 Ω cm, *B*	n-type 0.05 Ω cm, *P*	p-type 4 Ω cm, *B*	n-type 0.05 Ω cm, *P*
TCE_{S11}	64.73 ± 0.29	63.60 ± 0.60	61.19 ± 1.1	60.51 ± 0.35
TCE_{S12}	51.48 ± 1.5	45.79 ± 2.8	72.26 ± 5.1	75.70 ± 6.1
TCE_{S44}	60.14 ± 0.20	57.96 ± 0.17	54.90 ± 1.7	57.31 ± 1.4
TCE_{C11}	−73.25 ± 0.49	−74.87 ± 0.99	−49.26 ± 4.8	−45.14 ± 1.4
TCE_{C12}	−91.59 ± 1.5	−99.46 ± 3.5	−32.70 ± 10.1	−20.59 ± 11.0
TCE_{C44}	−60.14 ± 0.20	−57.96 ± 0.17	−51.28 ± 1.9	−53.95 ± 1.8

For simplified analyses, or analytic expressions, a single isotropic elasticity value may be used. To insure accuracy, the choice of this value must depend on the orientation and loading of the structure. Since the crystal structure of silicon has a cubic symmetry, computations in configurations presenting orthogonal shapes and loads will be reasonably accurate, as long as the appropriate elasticity value for the direction family is used. But for more complex cases with off-axis orientations or non-rectilinear structures, the use of the full orthotropic description will have significant benefits for the accuracy of the results.

Hardness

Hardness may be defined as the resistance of a material to permanent penetration by another material. The most important and comprehensive work about nanoindentation experiments to measure silicon hardness was performed by Bhushan et al. [31, 32]. Even though hardness values are dependent on the normal load, the indentation depth and crystallographic orientation, a value of 12 ± 1 GPa could be considered as average for all the cases. The only exception is a p-type silicon, boron-doped: it is shown that the doping using thermal diffusion with boron ions softened the silicon surface down to ∼7 GPa [32] .

Temperature effects on elastic constants

The silicon Young's modulus evolves with temperature. This thermal dependency is traditionally described for each elastic constant $C_{11}, C_{12}, S_{11}, \ldots$ with the thermal coefficient of elasticity (TCE) of the considered elastic constant. More precisely, for each of these constants C, its thermal variation between T_0 and T can be described via a power series of coefficients $\mathrm{TCE}(C)_k$:

$$C(T) = C(T_0)\left[1 + \sum_{k\geq 1} \mathrm{TCE}(C)_k (T - T_0)^k\right] \tag{10}$$

Several different measurements of TCE are reported in the literature [33–35] for the first-order temperature coefficients, and so their values cannot be given definitively. However, as recently reported by Hopcroft et al. [36], the results given by Bourgeois et al. [35] seem to come from the most carefully performed experiments as the values proposed include the second-order temperature coefficients (see Table 3).

Macroscopic mechanical behavior at high temperature

As stated before, beyond the elastic regime, silicon is a brittle material for low temperatures, but exhibits viscoplastic behavior before ductile failure above the brittle–ductile temperature T_{BD}. This viscoplastic behavior strongly depends on strain rate and temperature. At high temperature, the stress–strain curve of silicon shows two yield regions. Indeed after elastic domain, and between the upper yield stress and the lower yield stress, silicon exhibits a transient softening effect due to a drastic increase of dislocation density. Then, after the lower yield point, small and then strong work-hardening are observed (stage I and II). This behavior is classically modeled in the crystal plasticity framework, accounting for the discrete nature of plastic slip in crystal as in [37, 38], or in a more standard isotropic formulation of plastic flow as in [39, 40]. In the latest model, the plastic strain rate produced by a crystal ($\dot{\bar{\gamma}}^P$) is, in general, determined by the Orowan equation [41]:

$$\dot{\bar{\gamma}}^P = \rho_{\mathrm{m}} b \bar{v}, \tag{11}$$

where ρ_{m} is the mobile dislocations density which corresponds to a part of the statistically stored dislocations (SSDs) density [27, 42], b is the Burgers vector magnitude, and $\bar{v}$ is the average velocity of these dislocations. In accordance with experimental measurement, the dislocation velocity $\bar{v}$ is a function of the temperature T (Arrhenius factor) and of the effective shear stress τ_{eff} (power law)

$$\bar{v} = v_0 \left(\frac{\tau_{\mathrm{eff}}}{\tau_0}\right)^{1/m} \exp\left[\frac{-U_{\mathrm{dis}}}{kT}\right] \mathrm{sign}(\tau), \tag{12}$$

where v_0 and τ_0 are reference values for the dislocation velocity and stress, m is the stress exponent, k is the

Boltzmann's constant, and U_{dis} is the activation energy for dislocation velocity. The effective shear stress is the difference between the internal stress τ_i and the applied stress τ:

$$\tau_{eff} = \langle |\tau| - \tau_i \rangle, \quad \text{with } \langle x \rangle = \frac{x + |x|}{2}. \tag{13}$$

Then, the different constitutive models available in the literature are traditionally derived from the work of Alexander et al. [43], which is quite successful for initial stages of deformation up to the lower yield point. After this point, more appropriate models, like the ones proposed by Delaire et al. [44] or Moon et al. [40] are needed. In the Alexander and Haasen's model, the mobile dislocations density ρ_m is supposed to be equal to the total dislocation density ρ, and the internal stress τ_i is given by the following relation, where α is a constant, and μ is the shear modulus:

$$\tau_i = \tau_0 + \alpha \mu b \sqrt{\rho}. \tag{14}$$

The evolution equation for the dislocation density is finally described by the following equation, in which K is a material constant taken into account the creation and annihilation of the SSDs:

$$\dot{\rho} = \frac{K}{b} \tau_{eff} \dot{\bar{\gamma}}^P \tag{15}$$

Note that in the case of the Alexander and Haasen's model, the temperature and strain rate dependence of the upper τ_{uyp} and lower τ_{lyp} yield points are straightly described by:

$$\tau_{uyp/lyp} = C_{uyp/lyp} \dot{\bar{\gamma}}^{1/(2+m)} \exp\left[\frac{U_{dis}}{(2+m)kT}\right], \tag{16}$$

where $C_{uyp/lyp}$ are constants, respectively, associated to the upper and lower yield points. The following values for the different models constants, in case of undoped silicon, can be found in the literature (Table 4)

Thermal properties of single-crystal silicon

If thermal problems have to be faced, thermal conductivity (κ), diffusivity (D), specific heat (C_p), and emissivity (e) of silicon have to be known for different temperatures. If stresses induced by the change of temperature, i.e., thermal stresses, are of interest, also the CTE (α_T) must be evaluated.

Thermal conductivity, diffusivity, and specific heat

Above 200 K, the thermal conductivity is largely independent from the particular sample specification and the various reported data obtained through different methods show a rather good agreement [45–49]. The following values are representative measurements from Glassbrenner and Slack [46].

Concerning the thermal diffusivity D of single-crystal silicon, the values in Table 5 were measured from room temperature up to 1400 K by Abeles et al. [45]. These measurements were found in between those of Glassbrenner and Slack [46] and Shanks et al. [50] which are within the order of 5 % accurate below 1000 K, but less accurate above. Specific heat recommended data reported by Hull [51] are also given in Table 5.

From these previous experimental data, the conductivity can also be given by the following [52]:

$$\kappa = \kappa_0 \left[1 - B\left(\frac{T - T_0}{T}\right)^A\right], \quad \text{with} \begin{cases} B = 1.093 \text{ and } A = 0.7805 & T < 1000\,\text{K} \\ B = 0.93795 \text{ and } A = 0.42 & T > 1000\,\text{K} \end{cases}, \tag{17}$$

Table 5 Single-crystal silicon thermal conductivity (κ), diffusivity (D), and specific heat (C_p)

T (K)	κ (W cm^{-1} K^{-1})	D (cm^2 s^{-1})	C_p (J g^{-1} K^{-1})
200	2.66		0.557
300	1.56	0.86	0.713
400	1.05	0.52	0.785
500	0.80	0.37	0.832
600	0.64	0.29	0.849
700	0.52	0.24	0.866
800	0.43	0.19	0.883
900	0.356	0.16	0.899
1000	0.31	0.14	0.916
1100	0.28	0.13	0.933
1200	0.261	0.12	0.950
1300	0.248	0.12	0.967
1400	0.237	0.12	0.983
1500	0.227		1.000
1600	0.219		1.017

Table 4 Models constant values

b	v_0	τ_0	U_{dis}	m	α	K
3.83e^{-10} m	4.3e^{-4} m/s	5.5 MPa	2.35 eV	0.91	0.3–2.0	2e^{-4} m/N

where κ_0 is the thermal conductivity of silicon (W cm^{-1} K^{-1}) at room temperature T_0.

Emissivity

There have been several studies of the thermal radiation emitted by silicon at elevated temperatures. But since silicon emissivity strongly depends on many factors, such as the sample thickness, doping, surface conditions, etc., experiments must be interpreted with care before applying one of the various measured silicon emissivity values to any kind of model. As first approximation, an emissivity value acceptable regarding the different experimental results is null at room temperature, which then rises smoothly with temperature increase to a maximum value of 0.7 at 1220 K.

Thermal expansion

The single-crystal silicon thermal expansion coefficient α_T has been measured in the range 120 to 1500 K by several means such as an interferometric dilatometer [53, 54], X-ray diffractometry [55], and other techniques [56]. The reported measurements were found in good agreement between different methods (Table 6). From these measurements, a fitting expression of the linear thermal expansion coefficient $\alpha_T(10^{-6}\,\mathrm{K}^{-1})$ is given by [55]:

$$\alpha(T) = 3.725\left(1 - \mathrm{e}^{-5.88\times10^{-3}(T-124)}\right) + 5.548\times10^{-4}T \tag{18}$$

with T between 120 and 1500 K. At room temperature the recommended value is $\alpha(298.2) = 2.59 \pm 0.05\times 10^{-6}\,\mathrm{K}^{-1}$. Note that the effect of temperature on silicon density can also be evaluated from these values.

Table 6 Single-crystal silicon thermal expansion coefficient values

T (K)	χ (W cm^{-1} K^{-1})
300	2.616
400	3.253
500	3.614
600	3.842
700	4.016
800	4.151
900	4.185
1000	4.258
1100	4.323
1200	4.384
1300	4.442
1400	4.500
1500	4.556

Fracture properties of single-crystal silicon

Brittle–ductile transition

Single-crystal silicon is a brittle material at room temperature, in which cracks propagate without any appreciable plastic deformation. Nevertheless, it exhibits a ductile behavior above a certain temperature T_{BD}, for a given loading rate (or increase rate of stress intensity) and doping level. Single-crystal silicon brittle–ductile transition experiments were carried out especially by St. John [57], Brede and Haasen [58], Hirsch et al. [59–61], George and Michot [62], Hsia and Argon [63]. They pointed out that silicon presents a particularly sharp brittle–ductile transition. This transition is indeed associated with a sudden increase in stress to fracture, in order to intercept the yield stress curve. This transition occurs over a very narrow temperature range, typically less than 10 K (Fig. 1). The microscopic studies of the fractured samples have shown that there is hardly any dislocation activity at the crack tip below the brittle–ductile transition temperature, few hundred dislocations can be seen from the crack, moving into the bulk, along well-defined crystallographic directions approaching T_{BD} and a huge amount of dislocations nucleate above this critical temperature T_{BD}. It is also important to note that if silicon is pre-deformed to introduce dislocations and dislocations sources, it exhibits a softer transition [64].

Figure 2 illustrates the Arrhenius plot of the most current data on the brittle–ductile transition temperature. It shows that, although all the lines for intrinsic silicon have the same slope, the intercepts vary widely from one result to another, showing the dependence on the testing methods (especially levels of crack tip perfection). It also points out that p-type dopants do not affect the brittle–ductile transition temperature, while n-type dopants decrease it. Moreover, T_{BD} increases with a higher rate of stress intensity. These experiments have determined T_{BD} as a function of, using the activation energy for the

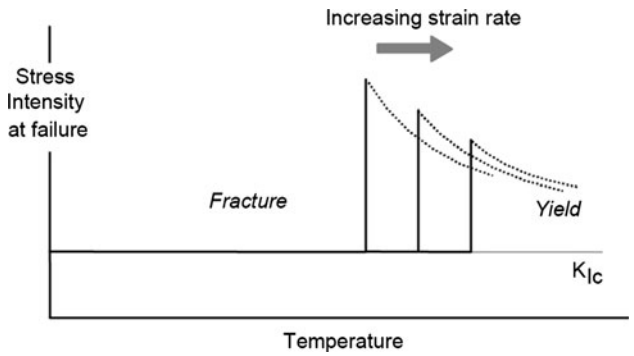

Fig. 1 Sharp brittle–ductile transition in silicon. The stress intensity at fracture rises abruptly at T_{BD}

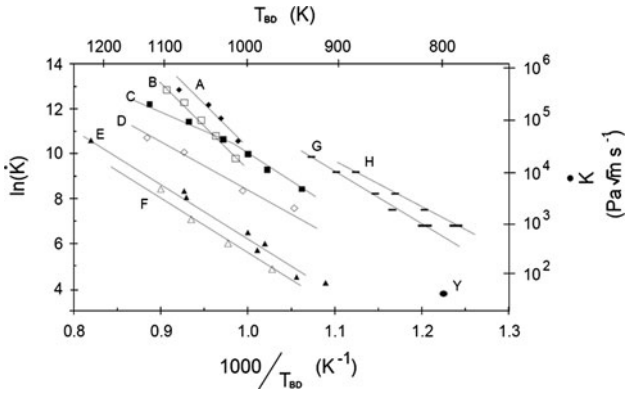

Fig. 2 Brittle–ductile transition temperature in silicon. Data from: ABC [58], D [57], EF [62], GH [59]. Doping levels: ABCH n-type, and DEFGH intrinsic

brittle–ductile transition U_{BD} (this activation energy was found to be nearly equal to U_{dis} in Eq. (12):

$$\dot{K} = A \exp\left(\frac{-U_{BD}}{kT_{BD}}\right), \tag{19}$$

where A is a model constant, and k is the Boltzmann constant. U_{BD} was measured to be 2.1 eV for intrinsic, and 1.6 eV for n-type silicon by Samuels and Roberts [59]. The most quantitative model proposed for the brittle–ductile transition in silicon is the one proposed by Hirsch and Roberts [61, 65]. In this model, the shielding of the crack front by dislocations emitted from there competes with the rise of the stress intensity factor K_I to the critical value K_{Ic}. The main feature of the model is that the material becomes ductile only when the emitted dislocations shield every point of the crack front. In this sense, the mobility of the dislocations plays the major role in this model.

Fracture toughness

As for the mechanical properties, the single-crystal silicon fracture toughness K_{Ic} depends on the crystallographic orientation. Vickers micro-hardness indentation associated, or not, with four point bending, and double-cantilever beam are the most commonly used methods to evaluate this toughness anisotropy. Since the different reported silicon fracture studies have emphasized the fracture anisotropy on the low index planes, we will focus here on the fracture toughness of these planes, i.e., {100}, {110}, and {111} planes, although many higher order index planes surface energy values sit between the ones of the low index planes [66]. These results suggest that silicon may also cleave on crystallographic planes other than the low index ones [67, 68]. Table 7 summarizes the fractures toughness and fracture energy values at room temperature reported in the literature. As seen in the previous section, these fracture

Table 7 Reported silicon fracture toughness and fracture energy values

Fracture planes	Fracture toughness K_{Ic} (MPa $m^{1/2}$)			Fracture energy γ_s (J m^2)		
	{111}	{110}	{100}	{111}	{110}	{100}
[69]	0.62					
[70]	0.62	0.71	0.75			
[57]	0.93					
[71]	0.82	0.90	0.95			
[72]	0.65	0.80				
[73]	1.00					
[74]		0.78				
[75]		1.05–1.19				
[76]	1.14–1.19	1.07–1.18	0.82–1.15			
[77]		0.95				
[68]	1.22	0.81–1.01	0.86–1.25			
[78]	0.66					
[79]		0.68–0.73				
[80]		1.15				
[81]		1.12	1.29			
[82]		0.63–0.74	1.11			
[83] (DFT)					1.73	1.73
[84] (MD)				1.19	1.50	2.26
[85] (DFT)						1.56
[86] (MD)	0.656			1.45		
[86] (DFT)	0.646					

MD Molecular dynamics, *DFT* density functional theory

toughness values are valid for temperatures below the brittle–ductile transition one. In case of simulated values, the method is written in parentheses: molecular dynamics (MD) or density functional theory (DFT).

The referenced articles might report values either in terms of fracture surface energy $\gamma_{(hkl)}$ or fracture toughness $K_{\mathrm{Ic}(hkl)}$. The following approximate equation, in which $E_{[hkl]}$ is the Young's modulus in the perpendicular direction to the crack surface, was used to convert them when necessary:

$$K_{\mathrm{Ic}(hkl)} = \left(2\gamma_{(hkl)}E_{[hkl]}\right)^{1/2}. \quad (20)$$

As first remark, the countervailing maxima and minima in the modulus and fracture resistance variations lead to a very small variation in toughness with fracture planes. Silicon is reported to have two principal cleavage planes: {111} planes, usually the easiest cleavage plane and {110} planes. In other words, the cleavage energy of {111} is lower than {100} one and thus, crack will unlikely propagate on the {100} plane.

Different crack propagation directions have been studied for both fracture planes. The ⟨110⟩ propagation directions were seen to be the preferred propagation directions on both cleavage planes. Nevertheless, on the {111} fracture surface, the anisotropy with respect to propagation direction manifests itself only in faint markings along ⟨110⟩ directions. Complementary, cleavage fracture on the {110} plane is very anisotropic. Propagation along the ⟨110⟩ directions is easy and results in nearly perfectly flat fracture surfaces, while along the ⟨110⟩ directions, perpendicular to the preferred direction, the crack deflects onto {111} planes inclined by 35.26° with respect to the original fracture plane [68, 75, 87]. In contrast to the results of the {110} fracture planes, the cracks introduced along the {100} planes were observed to deviate from these planes. These results can be understood by the fact that the fracture toughness of the {100} planes is almost the same as those of the higher order planes near {100}. Cracks following the {100} planes even deflect onto {110} planes, inclined by 45° with respect to the {100} planes, since these second planes exhibit the minimum fracture toughness value among the possible deflecting planes [81, 84].

Aside, there is an experiment of Deegan et al. [88] who observed that cracks which deviate from the ⟨110⟩ plane can travel in arbitrary directions, moreover these directions can fluctuate wildly creating a fractal fracture surface. This influence of the crack propagation direction in a given fracture plane, and the fact that cracks often deflect from the original fracture plane, are therefore responsible for the large scatter in the measured toughness value for each fracture plane, as clearly pointed out in Table 7. Many other parameters contribute to this scatter, including the testing method, specimen surface preparation, and the crack length measurement in case of indentation fracture method.

Even though some ambiguities exist in the literature regarding the exact value of the fracture toughness of single-crystal silicon, it appears that the earliest measurements of silicon fracture toughness [69, 70], using the well-defined double-cantilever beam geometry, are the least ambiguous from a testing geometry perspective, and in best agreement [89] with both MD calculations, based on known bond-rupture energies, and experimental scaling of fracture resistance with band-gap in elemental and compound semiconductors. Over the past 40 years, subsequent measurements using smaller cracks from indentation fractographic methods seem to always overestimate fracture toughness while providing critical information on the orientation dependence of fracture toughness. In Table 8 is summarized the range of values reported for fracture toughness and fracture energy and some recommended values based on aforementioned considerations. Both values for fracture toughness and fracture energy are reported for reader's convenience, using Eq. (20) to convert them.

Crack speed

The development of high-speed data acquisition has extended studies to dynamic crack propagation at crack driving forces greater than the equilibrium fracture resistance. Different experiments [78, 90–93] show that cracks propagate with velocities of about 1–5 km s^{-1}. There is therefore an apparent *speed gap* between 0 and ~1–2 km s^{-1} for crack driving forces just exceeding the fracture resistance [94, 95].

A possible explanation of this phenomenon is described by many scholars [96–98] and recently by Bernstein and

Table 8 Summary of reported and recommended silicon fracture toughness and fracture energy values

Fracture planes	{111}	{110}	{100}
Reported experimental range Fracture toughness K_{Ic} (MPa $m^{1/2}$)	0.62–1.22	0.68–1.19	0.75–1.29
Reported simulated range Fracture energy γ_s (J m^2)	1.19–1.45	1.50–1.73	1.56–2.26
Recommended value Fracture toughness K_{Ic} (MPa $m^{1/2}$)	0.62	0.71	0.75
Recommended value Fracture energy γ_s (J m^2)	1.022	1.483	2.163

Hess [99] where they indicate the presence of lattice trapping barriers as major player for the propagation of a brittle fracture, i.e., the fracture crack might lead to a configuration where the stress could be below or above the Griffith stress but the crack is stable [96].

Deegan et al. [88] report that, depending on the speed of the crack propagation, transitions from straight to wavy to multiply branched cracks are possible and could be discontinuous, bistable, and hysteretic. At large crack driving forces, the velocities approach an apparent upper limit approximately equal to 75 % of the Rayleigh wave speed $c_R \sim 4.6$ km s^{-1} depending on the direction of crack propagation [100, 101].

Conclusion

Single-crystal silicon has been extensively used in the electronic industry, and therefore numerous studies have also been performed and most of the needed parameters for the computation are available in the literature. These data have been gathered and compared here for a large temperature range.

Due to its crystalline structure, silicon is a strongly anisotropic material whose properties depend on orientation relative to the crystal lattice, especially regarding its fracture behavior. Several toughness values have been found in the literature. However the variation of fracture toughness between each orientation planes remains small.

More importantly, silicon is a brittle material at room temperature, which means that its behavior is purely elastic until it fails. But it also exhibits a sharp brittle–ductile transition at a precise temperature.

Acknowledgments The authors wish to thank EC for the financial support for this research (SUGAR Project FP7 No. 256752). A special thanks to Guillaume Lebret.

References

1. Gordon I, Dross F, Depauw V, Masolin A, Qiu Y, Vaes J, Van Gestel D, Poortmans J (2001) Sol Energy Mater Sol Cells 95(Suppl 1):S2
2. Henley FJ (2010) In: 35th IEEE photovoltaic specialists conference (PVSC), IEEE, pp 001184–001192
3. Masolin A, Recaman Payo M (2012) WO/2012/034993
4. Hillberry BM (1975) US 3,901,423
5. Wilkes DF (1981) US 4,244,348
6. Tanielian M, Lajos R, Blackstone S (1986) US 4,582,559
7. Owens G (2005) WO/2005/122243
8. Owens G (2010) EP1782465
9. Takeguchi M, Yamamoto T, Nakano M (1990) US 4,955,357
10. Yamaguchi S (2008) US 7,351,282
11. Baer SC (2009) US 2009/0056513
12. Dross F, Robbelein J, Vandevelde B, Van Kerschaver E, Gordon I, Beaucarne G, Poortmans J (2007) Appl Phys A 89:149
13. Dross F, Van Kerschaver E, Beaucarne G (2007) EP1863100
14. Dross F, Van Kerschaver E, Beaucarne G (2011) US 7,875,531
15. Qian J, Kersschot B, Masolin A, Vaes J, Frederic D, Reynaerts D (2011) In: 11th international conference of Euspen, vol 2, p 435
16. Vaes J, Masolin A, Pesquera A, Dross F (2010) In: Proceedings of SPIE, vol 7772, p 777212
17. Masolin A, Vaes J, Dross F, Poortmans J, Mertens R (2010) In: 35th IEEE photovoltaic specialists conference (PVSC), IEEE, p 002180
18. Masolin A, Vaes J, Dross F, Martini R, Rodriguez A, Poortmans J, Mertens R (2011) MRS Online Proc Libr 1323
19. Martini R, Masolin A (2012) Energy Proc 20
20. Mathew L, Jawarani D (2010) US 7,749,884
21. Rao RA, Mathew L, Saha S, Smith S, Sarkar D, Garcia R, Stout R, Gurmu A, Onyegam E, Ahn D, Xu D, Jawarani D, Fossum J, Banerjee S (2011) In: Photovoltaic specialists conference (PVSC), 2011 37th IEEE, p 001504
22. Bedell SW, Fogel KE, Lauro PA, Sadana D, Shahrjerdi D (2010) US 2010/0310775
23. Bedell SW, Fogel KE, Lauro PA, Sadana D, Shahrjerdi D (2011) WO/2011/106203
24. Bedell S, Shahrjerdi D, Hekmatshoar B, Fogel K, Lauro P, Ott J, Sosa N, Sadana D (2012) Photovoltaics 2:141
25. Mason WP (1958) Physical acoustics and the properties of solids. Van Nostrand, Princeton
26. Hall J (1967) Phys Rev 161(3):756–761
27. Nye JF, Lindsay RB (1957) Phys Today 10(12):26
28. Brantley WA (1973) J Appl Phys 44:534
29. Balamane H, Halicioglu T, Tiller WA et al (1992) Phys Rev B 46(4):2250
30. Haynes PD (1998) PhD thesis, Christ's College, Cambridge
31. Bhushan B, Koinkar VN (1994) Appl Phys Lett 64:1653
32. Bhushan B, Li X (1997) J Mater Res 12(1):54
33. McSkimin H, Bond W, Buehler E, Teal G (1951) Phys Rev 83(5):1080
34. Burenkov YA, Nikanorov SP (1974) Sov Phys Solid state 16(5):1496
35. Bourgeois C, Steinsland E, Blanc N, de Rooij NF (1997) In: Frequency control symposium. Proceedings of the 1997 IEEE International, p 791
36. Hopcroft M, Nix W, Kenny T (2010) J Microelectromech Syst 19:229
37. Cacho F, Orain S, Cailletaud G, Jaouen H (2007) Microelectron Reliab 47:161
38. Cochard J, Yonenaga I, Gouttebroze S, MHamdi M, Zhang ZL (2010) J Appl Phys 107:033512
39. Dillon OW, Tsai CT, De Angelis RJ (1986) J Appl Phys 60:1784
40. Moon H, Anand L, Spearing S (2001) MRS Online Proc Libr 687, Paper B9.6
41. Orowan E (1940) Proc Phys Soc 52:8
42. Arsenlis A, Parks D (1999) Acta Mater 47:1597
43. Alexander H, Haasen P, Frederick Seitz DT, Ehrenreich H (1969) Solid State Phys 22:27
44. Delaire F, Raphanel J, Rey C (2000) Acta Mater 48:1075
45. Abeles B, Beers DS, Cody GD, Dismukes JP (1962) Phys Rev 125:44
46. Glassbrenner C, Slack G (1964) Phys Rev 134(4A):A1058
47. Fulkerson W, Moore JP, Williams RK, Graves RS, McElroy DL (1968) Phys Rev 167:765
48. Yamamoto K, Abe T, Takasu S (1991) Jpn J Appl Phys 30(1):2423
49. Yamasue E, Susa M, Fukuyama H, Nagata K (2002) J Cryst Growth 234(1):121
50. Shanks H, Maycock P, Sidles P, Danielson G (1963) Phys Rev 130(5):1743

51. Hull R (1999) Properties of crystalline silicon. IET, London
52. Prakash C (1978) Microelectron Reliab 18(4):333
53. Okaji M (1988) Int J Thermophys 9(6):1101
54. Watanabe H, Yamada N, Okaji M (2004) Int J Thermophys 25(1):221
55. Okada Y, Tokumaru Y (1984) J Appl Phys 56(2):314
56. Swenson CA (1983) J Phys Chem Ref Data 12:179
57. St. John C (1975) Phil Mag 32(6):1193
58. Brede M, Haasen P (1988) Acta Metall 36:2003
59. Samuels J, Roberts S (1989) Proc R Soc Lond Ser A 421(1860):1
60. Hirsch P, Roberts S, Samuels J (1989) Proc R Soc Lond Ser A 421(1860):25
61. Hirsch P, Roberts S (1991) Philos Mag A 64(1):55
62. George A, Michot G (1993) Mater Sci Eng A 164(1–2):118
63. Hsia K, Argon A (1994) Mater Sci Eng A 176(1–2):111
64. Warren P (1989) Scripta Metall 23(5):637
65. Hirsch P, Roberts S (1997) Philos Trans R Soc Lond Ser A 355(1731):1991
66. Hesketh P, Ju C, Gowda S, Zanoria E, Danyluk S (1993) J Electrochem Soc 140:1080
67. Ebrahimi F, Hussain S (1995) Scripta Metall Mater 32(9):1507
68. Ebrahimi F, Kalwani L (1999) Mater Sci Eng A 268(1):116
69. Gilman J (1960) J Appl Phys 31(12):2208
70. Jaccodine R (1963) J Electrochem Soc 110:524
71. Chen CP, Leipold MH (1980) Appl Phys Lett 87(14):141912
72. Messmer C, Bilello J (1981) J Appl Phys 52(7):4623
73. Chen CP, Leipold MH (1986) In: Crack growth in single-crystal silicon. Plenum Press, New York, p 285
74. Bhaduri S, Wang F (1986) J Mater Sci 21(7):2489. doi:10.1007/BF01114295
75. Tsai Y, Mecholsky J (1991) J Mater Res 6(6):1248
76. Hayashi K, Tsujimoto S, Okamoto Y, Nishikawa T (1991) J Soc Mater Sci Jpn 40(451):405
77. Xin Y, Hsia K (1996) Acta Mater 44(3):845
78. Hauch J, Holland D, Marder M, Swinney H (1999) Phys Rev Lett 82(19):3823
79. Swadener J, Nastasi M (2002) J Mater Sci Lett 21(17):1363
80. Fitzgerald A, Iyer R, Dauskardt R, Kenny T (2002) J Mater Res 17(3):683
81. Tan J, Li S, Wan Y, Li F, Lu K (2003) Mater Sci Eng B 103(1):49
82. Cook RF (2006) J Mater Sci 41(3):841. doi:10.1007/s10853-006-6567-y
83. Pèrez R, Gumbsch P (2000) Acta Mater 48(18–19):4517
84. Tanaka M, Higashida K, Nakashima H, Takagi H, Fujiwara M (2006) Int J Fract 139(3):383
85. Ding Z, Zhou S, Zhao Y (2004) Phys Rev B 70:184117
86. Zhu T, Li J, Yip S (2004) Phys Rev Lett 93:205504
87. Perez R, Gumbsch P (2000) Phys Rev Lett 84(23):5347
88. Deegan RD, Chheda S, Patel L, Marder M, Swinney HL, Kim J, de Lozanne A (2003) Phys Rev E 67:066209
89. Clarke DR (1992) In: Faber KT and Malloy K (eds) Semiconductors and semimetals. Elsevier, Amsterdam, p 79
90. Cramer T, Wanner A, Gumbsch P (1997) Phys Status Solidi A 164:R5
91. Cramer T, Wanner A, Gumbsch P (2000) Phys Rev Lett 85:788
92. Sherman D, Be'ery I (2004) J Mech Phys Solids 52(8):1743
93. Sherman D (2005) J Mech Phys Solids 53(12):2742
94. Fineberg J, Marder M (1999) Phys Rep 313:1
95. Holland D, Marder M (1999) Adv Mater 11:793
96. Thomson R, Hsieh C, Rana V (1971) J Appl Phys 42:3154
97. Lawn BR (1975) J Mater Sci 10:469. doi:10.1007/BF00543692
98. Marder M (1999) Comput Sci Eng 1:48
99. Bernstein N, Hess DW (2003) Phys Rev Lett 91:025501
100. Coufal H (1994) J Acoust Soc Am 95(2):1158
101. Xu Y, Aizawa T (1999) Phys Lett A 260(6):512